Succinate in the tumor microenvironment affects tumor growth and modulates tumor associated macrophages

Sahil Inamdar [a], Abhirami P. Suresh [b], Joslyn L. Mangal [b], Nathan D. Ng [c], Alison Sundem [a], Hoda Shokrollahzadeh Behbahani [a], Thomas E. Rubino Jr. [d,e], Jordan R. Yaron [b], Taravat Khodaei [g], Matthew Green [a,h], Marion Curtis [d,e,f], Abhinav P. Acharya [a,b,g,h,i,j,*]

[a] *Chemical Engineering, School for the Engineering of Matter, Transport, and Energy, Arizona State University, Tempe, AZ, 85281, USA*
[b] *Biological Design, School for the Engineering of Matter, Transport, and Energy, Arizona State University, Tempe, AZ, 85281, USA*
[c] *Molecular Biosciences and Biotechnology, The College of Liberal Arts and Sciences, Arizona State University, Tempe, AZ, 85281, USA*
[d] *Department of Immunology, Mayo Clinic, Scottsdale, AZ, 85259, USA*
[e] *Department of Cancer Biology, Mayo Clinic, Scottsdale, AZ, 85259, USA*
[f] *College of Medicine and Science, Mayo Clinic, Scottsdale, AZ, 85259, USA*
[g] *Biomedical Engineering, School of Biological and Health Systems Engineering, Arizona State University, Tempe, AZ, 85281, USA*
[h] *Materials Science and Engineering, School for the Engineering of Matter, Transport, And Energy, Arizona State University, Tempe, AZ, 85281, USA*
[i] *Biodesign Center for Immunotherapy, Vaccines and Virotherapy, Arizona State University, Tempe, AZ, 85281, USA*
[j] *Department of Biomedical Engineering, Case Western Reserve University, Cleveland, OH 44106, United States*

Corresponding author. 550 GWC 651 E, Tyler Mall, Tempe, AZ, USA.
E-mail address: abhi.acharya@asu.edu (A.P. Acharya).

ARTICLE INFO

Keywords:
Succinate
Immunometabolism
Macrophages
Melanoma
Cancer

ABSTRACT

Succinate is an important metabolite that modulates metabolism of immune cells and cancer cells in the tumor microenvironment (TME). Herein, we report that polyethylene succinate (PES) microparticles (MPs) biomaterial mediated controlled delivery of succinate in the TME modulates macrophage responses. Administering PES MPs locally with or without a BRAF inhibitor systemically in an immune-defective aging mice with clinically relevant $BRAF^{V600E}$ mutated YUMM1.1 melanoma decreased tumor volume three-fold. PES MPs in the TME also led to maintenance of M1 macrophages with up-regulation of TSLP and type 1 interferon pathway. Impressively, this led to generation of pro-inflammatory adaptive immune responses in the form of increased T helper type 1 and T helper type 17 cells in the TME. Overall, our findings from this challenging tumor model suggest that immunometabolism-modifying PES MP strategies provide an approach for developing robust cancer immunotherapies.

1. Introduction

Immune cell responses modulating technologies have achieved great success in clinics and in basic science research [1–4]. Importantly, in the TME macrophages are important innate immune cells, and modulate cancer cell growth via phagocytosis and directing adaptive immune responses [5–9]. Notably, in several cancer types macrophages infiltrate and form majority of the immune cells in the TME [5,6]. Therefore, these cells form an important target in the TME to direct anti-cancer responses. Macrophages are broadly classified as having pro-inflammatory phenotype, which are referred to as M1 macrophages in this manuscript, which have anti-cancer properties. On the other hand, macrophages with anti-inflammatory phenotypes, which are referred to as M2 macrophages in this manuscript have pro-cancer properties. Therefore, increasing the ratio of M1/M2 macrophages can potentially skew the immune responses toward anti-cancer responses [10–12].

In addition to challenging issues of M2 macrophages mediated immunosuppression in the TME, aging represents another major challenge for cancer treatment. Aging is associated with decreased T cell based adaptive immune responses due to thymic involution, and a diminished ability to respond to M1 macrophage stimuli [13]. Moreover, it has been demonstrated that targeting macrophage activation in aging immune system can be effective in generating tumor regression in old mice [14]. Despite their defective nature, the macrophages in aging mice, also infiltrate the TME, where the cancer cells and immune cells compete for nutrients.

One of the key nutrients in the TME is succinate, which is generated in the Krebs cycle [15]. Notably, succinate has been associated with an inflammatory response and cancer cells also produce this metabolite intracellularly to activate HIF1a pathways [16,17]. Macrophages (Mϕs) express receptors called SUCNR1 which can then internalize this metabolite [18]. It has been demonstrated that succinate is directly linked to production of inflammatory cytokines IL-1β secretion, an effect that was lost in SUCNR1-deficient mice [16,19,20]. Therefore, extracellular delivery of succinate in the TME may have an inflammatory effect and generate pro-inflammatory immunotherapy [21]. Mϕs are innate cells and can sample particulate matter in the TME, which can then modulate their responses based on the nature of these particles [22,23]. Therefore, biomaterials that can deliver succinate to these phagocytic cells may be able to modulate immune-cell function [23,24].

This study describes a strategy for sustained release of succinate from particles, which allow Mϕs to perform their function even in the presence of chemotherapeutics in an aging immune system. Administration of such biomaterials in an aging mouse with clinically relevant $BRAF^{V600E}$ mutated YUMM1.1 melanoma decreased tumor volume threefold. Overall, this investigation develops new biomaterials with immunomodulatory properties for cancer treatment using simple metabolites.

2. Results and discussion

Mϕs can form a large portion of the tumor microenvironment [25] and play an important role in directing immune responses. To modulate the TAMs' phenotype and to avoid phagocytic cells' trafficking of PES MPs away from the tumor site >20 μm PES MPs were used (Fig. 1a and b). Aged mice (>65 weeks of age) were injected with both smaller and larger particles, containing IR783 fluorescent dye, contralaterally in the back. A significantly higher signal from the injection site of larger PES MPs was observed on day 2 (~1.5-fold) and day 3 (~1.3-fold) as compared to the injection sites of smaller PES MPs particles, suggesting faster trafficking of the smaller PES MPs (Supplementary Fig. S1). Hence, >20 μm PES MPs were used. To understand if PES MPs can release succinate, they were incubated in 1X PBS and the supernatant was analyzed using high-performance liquid chromatography. It was observed that the PES MPs were able to release free succinate in a sustained manner (Supplementary Fig. 1). Next, confocal microscopy was used to investigate Mϕs' ability to interact with the PES MPs. After 48 h of treatment with PES MPs, it was observed that multiple Mϕs were able to interact with these particles *in vitro* (Supplementary Fig. S2). Finally, the immunomodulatory effects of >20 μm PES MPs and PLX4720, a potent BRAF inhibitor, on the bone marrow-derived Mϕ phenotype was tested *in vitro*. Notably, when Mϕs were treated with PLX4720, the M1/M2 Mϕ ratio ($CD80^+C86^+$ of F4/80 to $CD206^+CD163^+$ of F4/80) significantly decreased as compared to untreated Mϕs (Fig. 1d). Moreover, the M1/M2 ratio of the Mϕ phenotype significantly increased when Mϕs were treated with PES MPs along with PLX4720, a BRAF inhibitor used in clinic for melanoma treatment (Fig. 1d). Although PES MPs were able to significantly increase the ratio of M1/M2 Mφs as compared to PLX4720, this ratio was not significantly different than no treatment control (p-value = 0.11). Overall, these data suggest that >20 μm PES MPs will be able to maintain a M1 Mϕs population even in the presence of PLX4720.

BRAF inhibition does lead to reduction in tumor growth in mice and humans, however the effect of BRAF inhibition on YUMM1.1, a model melanoma cell line needs to be evaluated. Therefore, IC50 values of PLX4720, a BRAF inhibitor against YUMM1.1 cells was determined. It was observed that the IC50 for PLX4720 in YUMM1.1 cells was 0.713 μM *in vitro* (Supplementary Fig. S3).

To test if PES MPs can modulate innate immune cells for melanoma treatment, a challenging melanoma model in an aging innate immune system was chosen. Notably, melanoma is most frequently diagnosed in aging populations (median age: 65) where naïve T-cell population is

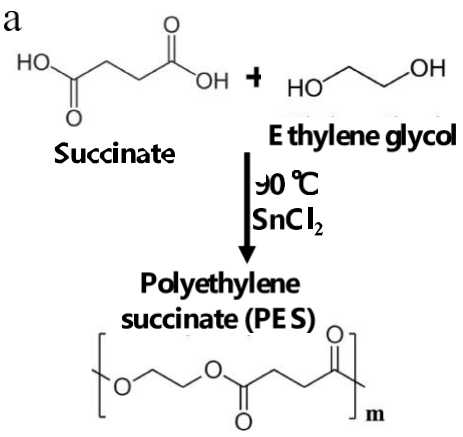

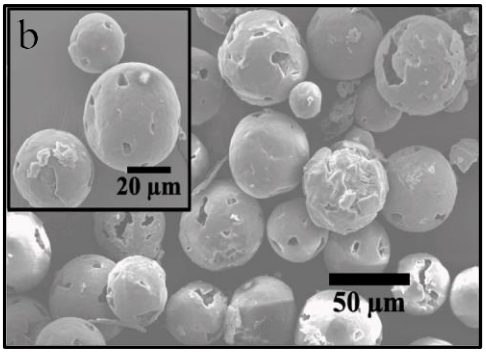

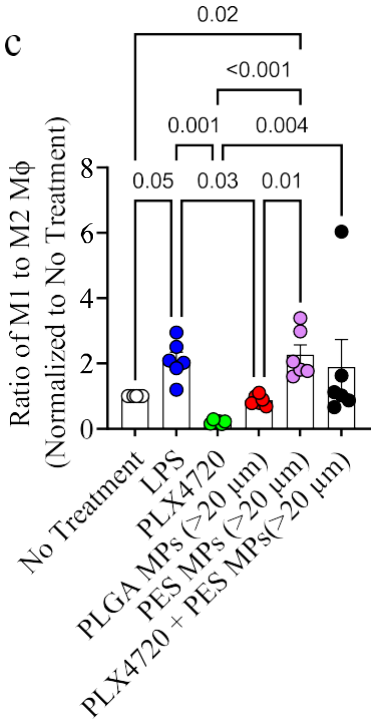

Fig. 1. PLX4720 decreases M1/M2 ratio of Mφs, and PES MPs (>20 μm) reinstates this ratio *in vitro*. (a) A schema of chemical synthesis of PES polymer. (b) PES MPs scanning electron microscopy image. (c) Significant decrease in M1/M2 ratio ($CD80^+C86^+$ of F4/80 to $CD206^+CD163^+$ of F4/80) was observed in Mφs treated with PLX4720 as compared to untreated Mφs, suggesting that PLX4720 modifies Mφ function. PES MPs treated Mφs in the presence of PLX4720 increase M1/M2 ratio ($CD80^+C86^+$ of F4/80 to $CD206^+CD163^+$ of F4/80) at the same level as LPS. (n = 6 for all groups; ns = no significance).

reduced and the ability to protect against cancer is diminished [26,27]. Interestingly, although innate immune cells are also functionally defective in the aging system, their overall population is not diminished as compared to younger population, and therefore, may be functionally modified to become effective in reducing tumor growth in aging immune system [28,29]. Contrarily, checkpoint inhibitor treatment is better in reducing tumor growth as compared to the younger immune system, and this was dependent on higher CD8:Treg ratios in aging immune system [30,31]. It is important to take into account both pro- and anti-inflammatory T cell phenotypes in the TME when developing an immunotherapy combined with chemotherapy.

To test local innate cells' ability to modulate tumor growth, tumors were contralaterally installed in mice, and the particles were added during tumor induction. Furthermore, individual mice's immune systems can vary greatly as they age [29]. Therefore, the PES MPs' effect on tumor size as compared to the controls was studied in the same mice. In this study, aged mice (>18 months old) were injected with YUMM1.1 ($BRAF^{V600E}$ mutated, mimics human melanoma mutation) murine melanoma cells along with PES MPs to determine innate immune cells' response to tumor growth (Fig. 2a). After administering the formulations *in vivo*, no significant changes in mouse weight were observed (Supplementary Fig. S4). Significant differences were observed from day 30 onwards in tumors injected with PES MPs as compared to untreated, soluble succinate-treated and control particles poly (lactic-*co*-glycolic) acid (PLGA) MP-treated tumors [32–34], indicating that PES MPs are able to reduce tumor growth by themselves (Fig. 2b). Also, a Seahorse assay was performed to study these particles' effect on YUMM1.1 cells' energy metabolism. No significant changes were observed in ECAR and OCR in these cells when incubated with PES MPs *in vitro*, indicating that these particles do not affect cancer-cell metabolism (Supplementary

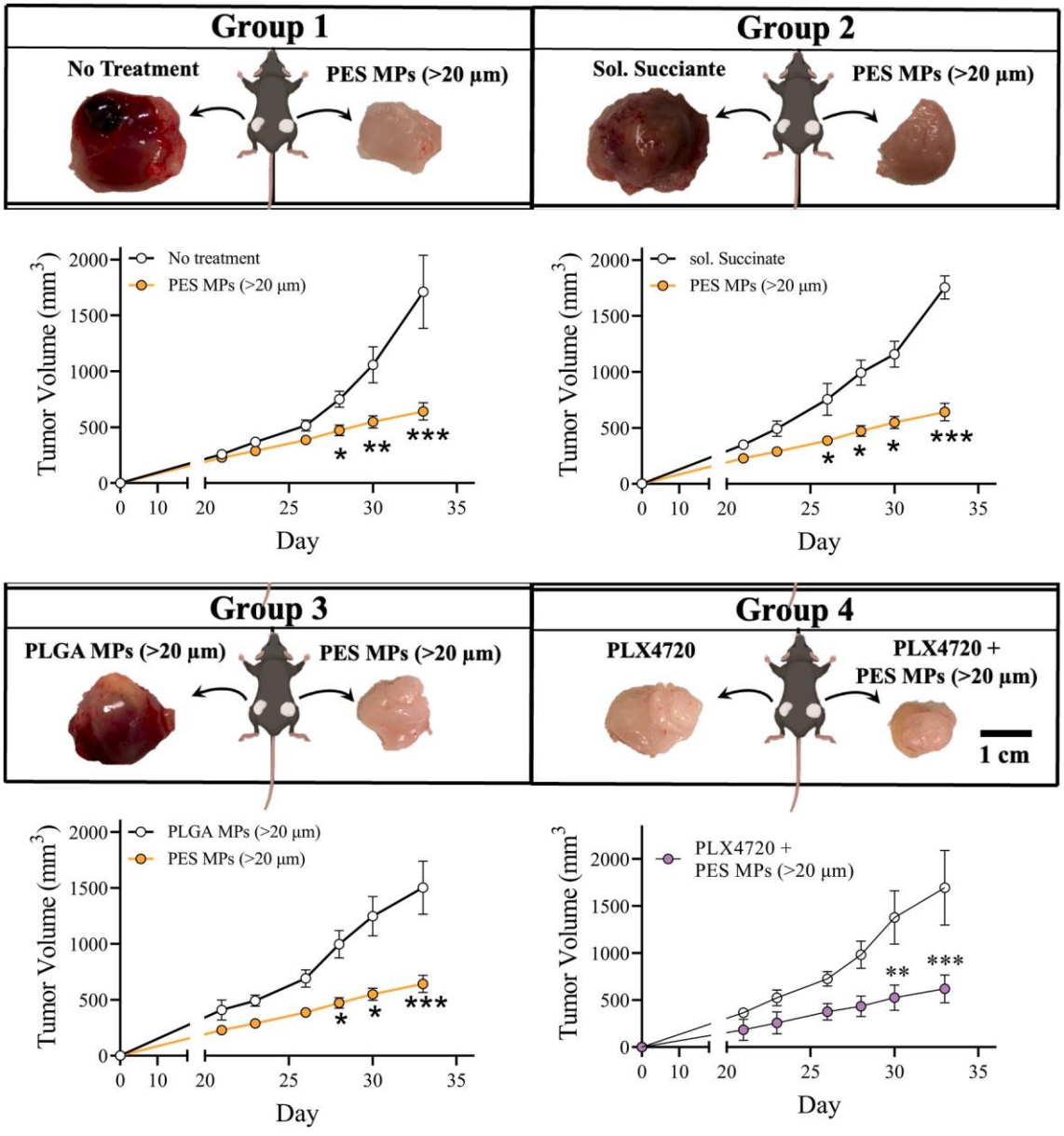

Fig. 2. PES MPs reduce tumor growth in aging immune-defective mice. Schematic of the treatment groups; Group I – left: No treatment, right: PES MPs; Group II – left: soluble succinate, right: PES MPs; Group III – left: PLGA MPs, right: PES MPs; Group IV – left: PLX4720, right: PLX4720 + PES MPs. Tumors treated with PES MPs grew significantly slower than untreated tumors or those treated with sol. Succinate or PLGA MPs (n = 3 per group; *p < 0.05, **p = 0.0037, ***p = 0.005, ****p=<0.0001; Two-way ANOVA). Tumors treated with PES MPs along with PLX4720 grew more slowly as compared to PLX4720-treated tumors. A significant reduction in tumors was seen from day 26 onwards in those treated with PLX4720 + PES MPs (n = 4 per group; *p < 0.05, **p = 0.0037,***p = 0.0002; Two-way ANOVA).

Fig. S5). Interestingly, tumors treated with PLX4720 along with PES MPs were significantly smaller as compared to those treated only with PLX4720, further confirming that PES MPs' presence in the tumor microenvironment (TME) influences tumor growth (Fig. 2c). Moreover, upon resecting the tumors, fibrous encapsulation of PES MPs was observed, which suggests that these particles might continue to release succinate beyond 33 days and modulate tumor growth.

Mice were sacrificed on day 33 post-tumor-induction to determine PES MPs' effect on the innate and adaptive immune system. In the spleen and inguinal lymph nodes, significant differences in the percentage populations of dendritic cells (DCs) another phagocyte, and Mϕs were observed (Supplementary Fig. S6). Also, there was a trend of increased levels of %CD80 + $CD86^+$ of F4/80+ innate cells in the spleen, cervical and inguinal lymph nodes, however these levels were not significantly different than the control of no treatment controls. A significant increase in activated DCs (MHC^+CD86^+ in $CD11c^+$), in the PES MP-treated tumors was observed as compared to untreated tumors and those treated with soluble succinate and PLGA MPs (Supplementary Fig. S7). Additionally, DCs and activated DCs significantly increased (~2-fold) in tumors treated with PES MPs + PLX4720 as compared to tumor treated with PLX4720 alone (Supplementary Fig. S7).

TAMs are pro-tumorigenic cell types; however, due to their malleable nature, they can potentially play an important role in reducing tumor growth [35,36]. Therefore, TAMs were isolated from the tumors on day 33 using a flow sorter ($CD45^+Ly6c^-Ly6G^-CD68^+F480^+$), and changes in RNA levels were studied using RNA-seq experiments (Fig. 3a). It was observed that the serglycin (*srgn*) gene and the TSLP pathway significantly increased in the TAMs isolated from the PES MP-treated tumors as compared to untreated tumors. Recent reports suggest that *srgn* encodes proteins associated with a macromolecular complex of granzymes. Moreover, a significant decrease in the TGB-β signaling pathway was observed in TAMs present in PES MP-treated tumors (Fig. 3b). TGB-β is one of the main immunosuppressive cytokines produced by TAMs in the tumor microenvironment [37]. Studies suggest that an increase in TGF-β can lead to increased expression of IL-10, another anti-inflammatory cytokine [38]. Therefore, a decrease in the TGB-β signaling pathway indicates reduced immunosuppression in TAMs present in the PES MP treatment group. Another interesting pathways that were upregulated in PES MPs treated TAMs, was regulation of type 1 interferon, regulation of microtubule polymerization and regulation of extracellular matrix organization. Taken together these pathways may allow for TAMs to chemotax around the tumor, and thus increase the likelihood of encountering cancer cells. Although, we observed downregulation of genes associated with TNFa pathway in PES MPs as compared to no treatment, these were not significantly decreased (Fig. 3c). Additionally, there was an increase in IL-6, a pro-inflammatory pathway, and IL-4, an anti-inflammatory pathway associated genes in PES MPs as compared to no treatment. Interestingly, prior studies have demonstrated that Type 2 immune responses generated due to extracellular matrix proteins, may support anti-tumor immune responses [39]. Moreover, it was identified that the RNA levels of *CD80* were upregulated in PES MP group, and there was no difference in RNA levels of *CD86*, which did not completely correlate with the flow cytometry data of activation due to PES MPs. However, if PES MPs are indeed leading to type 2 immunity mediated anti-tumor responses cannot be derived from these data directly, and further studies would be needed.

In addition, there was a significant increase in volume normalized number of Mϕs ($F4/80^+$) in the PES MP-treated tumors as compared to untreated tumors and those treated with soluble succinate and PLGA MPs (Fig. 4). Also, M1 Mϕs ($CD80^+CD86^+$ in $F4/80^+$) significantly increased (~4.5-fold), compared to untreated tumors and those treated with soluble succinate and PLGA MPs (Fig. 4b). The ratio of M1 Mϕs to M2 Mϕs ($CD163^+CD206^+$ of $F4/80^+$) significantly increased (~1.6-fold) compared to other treatment groups, which might indicate that tumor growth reduction is led by the pro-inflammatory, tumor-associated Mϕs (Fig. 4c). Furthermore, there was a significant increase in Mϕs as well as

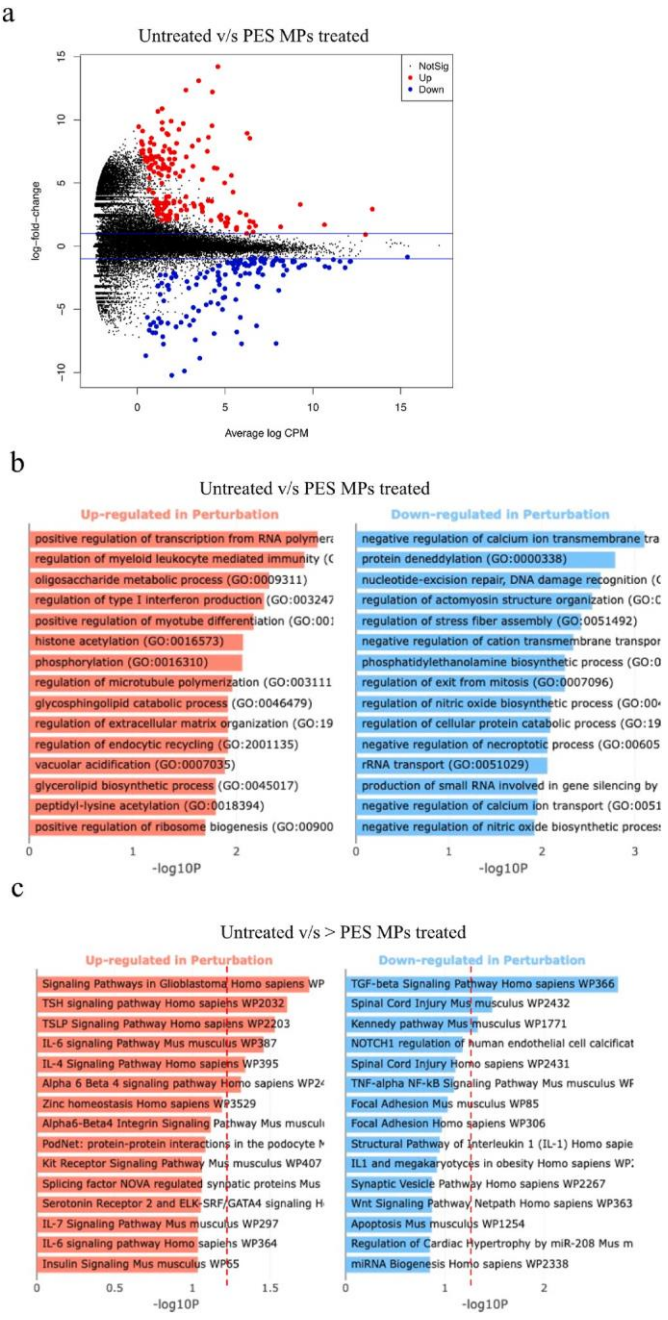

Fig. 3. PES MPs modulate macrophage RNA expression in the TME. a. Significant increase in the M1 phenotype was observed when TAMs isolated from PES MP-treated tumors were investigated using bulk RNA-seq as compared to untreated controls (n = 3; two-tailed unpaired Student's t-test, FC = fold change; P = p-value). The y-axis and x-axis are displayed as log2 bases. b,c. Significant changes using RNA-seq were observed in the pathways modified by PES MPs from tumor associated macrophages isolated from TME as compared to untreated control (n = 3; two-tailed unpaired Student's t-test; dashed red line indicates p = 0.05). The pathways that were altered were determined from the KEGG pathway (b) and Wikipathway (c) databases. Perterbuation = PES MPs.

M1 Mϕs in tumors treated with PES MPs + PLX4720 as compared to tumors treated with PLX4720 only (Fig. 4d and e). Overall, the ratio of M1 Mϕs to M2 Mϕs increased in tumors treated with PES MPs + PLX4720 as compared to tumors treated with the PLX4720 only (Fig. 4f), confirming the effect of PES MPs on pro-inflammatory TAMs associated with tumor growth reduction. Repolarization of TAMs to M1 phenotypic Mϕs has also been shown to significantly improve anti-tumor efficacies

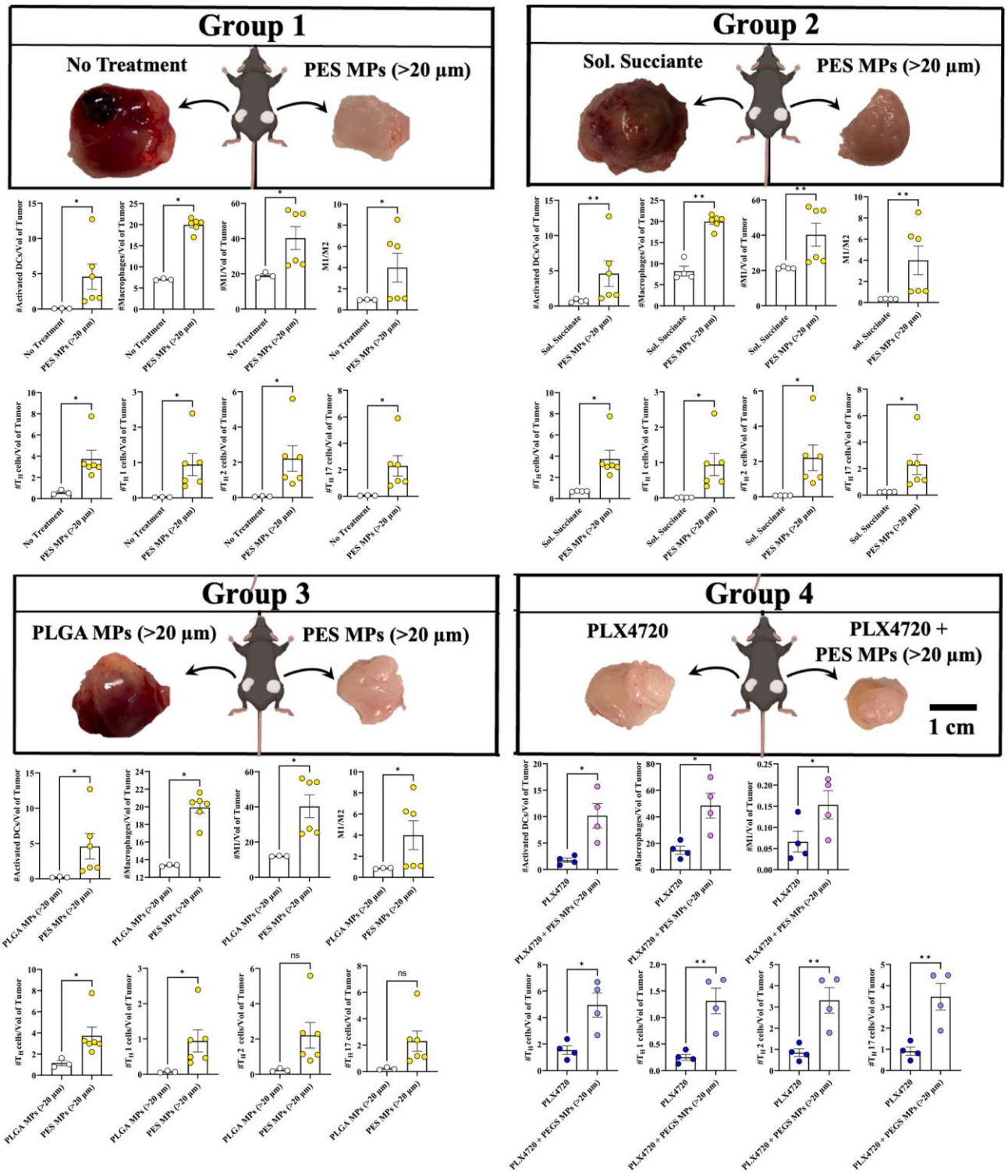

Fig. 4. PES MPs generate M1 innate cell and adaptive T cell responses in aging immune-defective mice. A significant increase in the tumor volume (vol) normalized number of activated DCs ($CD86^+CD80^+$ in CD11c+) total Mϕs (F4/80 in single cells), M1 Mϕs ($CD86^+CD80^+$ in F4/80+), and M1/M2 ratio ($CD80^+CD86^+$ in F4/80/CD163 + CD206+ in F4/80) was observed in tumors treated with PES MPs as compared to contralateral tumors treated with (Group 1) no treatment; (Group 2) soluble succinate; (Group 3) PLGA MPs; and (Group 4) PLX4720 (two-tailed unpaired Student's t-test). Significantly higher T_h, T_{h1}, T_{h2}, and T_{h17} cells was observed in tumors treated with PES MPs as compared to (Group 1) no treatment, and (Group 2) sol. Succinate and (Group 4) PLX4720; higher T_h, and T_{h1} against (Group 3) PLGA MPs (two-tailed unpaired Student's t-test). All the units of the y-axis are cells/mm^3. All data depicted as average ± std error.

in aggressive melanoma models [37].

Mice sacrificed on day 33 post-tumor-induction were also used to analyze the T-cell phenotype in lymph nodes and tumors (Fig. 4; Supplementary Figure S8). In the spleen and the inguinal and cervical lymph nodes, no significant differences were observed between the helper T cells - T_h cells ($\%CD4^+$) and cytotoxic T cells - T_c cells ($\%CD8^+$) for all groups, indicating no systemic T-cell responses in these cell types (Supplementary Figure S8). However, number of T helper (T_h),

proliferating T_h, T_{h1} cells (Tbet$^+$ in CD4$^+$) and T_{h2} (GATA3$^+$ in CD4$^+$) significantly increased in tumors treated with PES MPs as compared to untreated tumors and those treated with soluble succinate and PLGA MPs (Fig. 4, Group 2). Importantly, there was a significant upregulation of number of T_{h17} cells (RORγT$^+$ in CD4$^+$) in tumors treated with PES MPs as compared to all other treatment groups (Fig. 4, Groups 1–3). Similarly, there was a significant increase in the T-cell populations in tumors treated with PES MPs + PLX4720 as compared to tumors treated with PLX4720 only (Fig. 4, Group 4). Overall, although the naïve T-cell population is severely diminished in the aging immune system, treatment with PES MPs was able to generate a higher adaptive response as compared to the control, thus stressing the PES MPs' alarmin nature.

Prior studies have demonstrated the importance of T helper responses in preventing tumor growth in mice and in humans. Interestingly, it was demonstrated that type 2 immune responses were essential for reducing tumor growth in mice, and providing long-term survival in humans [39,40]. These studies suggest that T helper cells expressing GATA3, and Tbet, both might play an important role in preventing cancer cell proliferation. Moreover, Th cells can express multiple transcription factors at the same time, (e.g. RORγT and Tbet), however, most often one of the transcription factor dominates and drives cytokine production [41,42]. In this study, the levels of transcription factors were studied, and provides an indication of Th responses, however, cytokine production from these cells will provide further evidence of lineage of these cells in the TME.

In conclusion, this study demonstrates that succinate-based microparticles activate Mϕs by potentially modifying the TSLP signaling pathways, regulating Type I interferon pathway while downregulating TGF-beta pathway in TAMs. Thus, the PES MPs can act as an adjuvant by modulating the pro-inflammatory signaling pathways in Mϕs to generate robust pro-inflammatory responses. Also, PES MPs generate a robust anti-cancer response, which is necessary for melanoma treatment in aging immuno-defective mice. In clinic, Aldara™ cream, which contains imiquimod (toll-like receptor 7 agonist) as the active ingredient is used as a topical treatment for melanoma. This treatment is often prescribed as an alternate day treatment after the surgery of tumor removal from the skin. We envision that PES MPs, which can allow for succinate release in a sustained manner, can then provide a one-time application by the physician, and allow for control of tumor growth *in situ*. Therefore, in future studies, we will test the long-term ability of PES MPs to reduce tumor growth in an aging immune system.

3. Materials and methods

3.1. Polymer synthesis

Succinic acid and ethylene glycol were mixed in a round-bottom flask at equimolar ratio. This mixture was stirred at 90 °C for 16 h under vacuum. The polymer was then precipitated in methanol solution. A rotary evaporator was used to evaporate the remaining methanol, and the polymers were dried under vacuum at room temperature for 48 h.

3.2. Microparticle generation

A standard oil-water emulsion method was utilized to generate MPs. A total of 50 mg of the PES polymer was dissolved in 1 mL of dichloromethane (DCM, Fischer Scientific, Pittsburgh, PA). The solution was then added to 10 mL of 2% polyvinyl alcohol (PVA) solution in nanopure water and homogenized at 10,000 rpm using a handheld homogenizer (DREMEL 8220) for 2 min. The resulting emulsion was added to a continuously stirred 50 mL solution of 1% PVA set at 400 rpm for up to 2 h to allow for DCM evaporation. Subsequently, the particles were washed 3 times by centrifuging at 2000 Gs for 5 min, removing supernatant and resuspending in nanopure water each time. The microparticles were then lyophilized and stored at −20 °C and used for subsequent experiments.

3.3. Particle size determination

The size of the PES MPs was determined by imaging using scanning electron microscopy (SEM) XL30 Environmental FEG - FEI at Erying Materials Center at Arizona State University.

3.4. HPLC

Release kinetics of succinate from PES MPs was determined by incubating 5 mg of MPs in 1 mL of phosphate buffered saline (PBS) at pH 7.4, in triplicates. The samples were placed on a rotisserie at 37 °C for 30 days. At each time point, the samples were centrifuged at 300 X Gs for 5 min. Post centrifugation, 800 μL of the supernatant was removed and stored in microcentrifuge tubes at −20 °C. A total of 1X PBS buffer (800 μL) was added to the original samples, and the process was continued for each time point. The amount of metabolite released was then determined by developing a new method in high-performance liquid chromatography (HPLC, Agilent Technologies, Santa Clara, CA). Specifically, the mobile phase of 50% methanol in water was used. A 50 μL of injection volume was utilized in a Hi-Plex H, 7.7 × 300 mm, 8 μm column. The flow rate of 0.1 mL/min was utilized, and the absorbance was determined using a UV detector at 190 nm. The area under the curve of the peaks observed at a time of 13 min was determined using the ChemStation analysis software as per manufacturer's directions.

3.5. Endotoxin measurement assay

ToxinSensor™ Chromogenic LAL Endotoxin Assay Kit (GenScript) was used to measure endotoxin levels in the synthesized PES MPs., and the endotoxin levels were found to be below the detection limit.

3.6. Macrophage isolation and culture

Bone marrow-derived Mϕs (BM Mϕs) were generated from 6-8-week-old female C57BL/6j mice in compliance with the protocol approved by Arizona State University (protocol number 19–1688 R) using a modified 10-day protocol [43,44]. Femur and tibia from mice were isolated and kept in wash media (DMEM/F-12 (1:1) with L-glutamine (VWR, Radnor, PA), 10% fetal bovine serum (Atlanta Biologics, Flowery Branch, GA) and 1% penicillin-streptomycin (VWR, Radnor, PA). The ends of the bones were trimmed, and bone marrow was flushed out with 5 mL wash media and made into a homogenous suspension. Red blood cells (RBC) were lysed by centrifuging the suspension and incubating in 3 mL of 1X RBC lysis buffer for 5 min on ice. The cell suspension was centrifuged and washed with 7 mL wash media before resuspension in DC media DMEM/F-12 with L-glutamine (VWR, Radnor, PA), composed of 10% fetal bovine serum, 1% sodium pyruvate (VWR, Radnor, PA), 1% non-essential amino acids (VWR, Radnor, PA), 1% pen- icillin–streptomycin (VWR, Radnor, PA), and L929 media. For Mϕs, L929 cells were cultured to confluency in a T-75 flask. The cells were centrifuged, and supernatant was used for preparing Mϕs media. Specifically, 70% cell culture media contained (DMEM/F-12 with L-glutamine (VWR, Radnor, PA), 10% fetal bovine serum, 1% sodium pyruvate (VWR, Radnor, PA), 1% non-essential amino acids (VWR, Radnor, PA), 1% penicillin–streptomycin (VWR, Radnor, PA) while the rest 30% was L929 supernatant. The cells were later seeded in a tissue culture treated T-75 flask (Day 0). On day 2, floating cells were collected, centrifuged, and resuspended in fresh media, respectively, and seeded on ultra-low attachment plates for 7 additional days. The media was changed every day until day 9. On day 9, cells from the ultra-low attachment plates were resuspended and 0.1×10^6 cells/well were seeded on suitable tissue culture plates for the desired experiments for 1 more day (until day 10) before treatment. Cells in the tissue culture plates were used for further experiments/treatment on day 10. The purity, immaturity and yield of Mϕs was verified via immunofluorescence staining and flow cytometry. Mϕs were isolated from at least 3 separate mice for each type

of experiment.

3.7. Confocal microscopy

On day 10, 0.1 million cells were seeded on a glass slide within 24 well plates and were incubated for 24 h in 37 °C [45]. The cells were then treated with fluorescently labelled FITC-PES MPs. The nucleus and cytoplasm were stained with DAPI and rhodamine-phalloidin, respectively. Samples were imaged with a Nikon C2 laser scanning confocal microscope using a 60X, oil-immersion lens with numerical aperture of 1.4. DAPI, and fluorescently labelled rhodamine-PES MPs were excited with 405 nm and 561 nm lasers respectively, coupled with appropriate blue and red channel-emission detection. Image dimensions were 1024 × 1024 pixels scanned with a digital zoom of 2X. Z-stacks were created in the same manner, with a step size of 0.25 μm between optical slices. Cells treated with FITC-PES MPs and untreated cells were used as negative imaging controls to identify the signal of interest. Laser intensity and detector gain were adjusted to eliminate background or autofluorescence and avoid pixel saturation. Elements, a Nikon software, was used to adjust the intensity scale, create orthogonal views, and convert images to 8-bit TIFF format.

3.8. Extracellular flux assays

Oxidation consumption rate (OCR) was measured using Seahorse Extracellular Flux XF-96) analyser (Seahorse Bioscience, North Billerica, MA. Briefly, 200,000 cells/well were seeded in Seahorse XF-96 plates and cultured [46–48]. Cells were treated with 50 μg/well PES, or no treatment control. After 24 h, for OCR, media was changed to unbuffered DMEM containing 2 mM glutamine, 1 mM pyruvate, and 10 mM glucose following sequential injections of oligomycin (2 mM), 7 Carbonyl cyanide-4 (trifluoromethoxy) phenylhydrazone (FCCP) (1 mM), and antimycin/rotenone (1 mM). The OCR after the injection of oligomycin was a measure of ATP-linked respiration and the OCR after the injection of FCCP represented maximal respiratory capacity. Basal respiration was quantified by measuring OCR prior to the injection of oligomycin. All samples were analyzed with 6 technical replicates.

3.9. RNA-seq

Using KAPA's mRNA HyperPrep Kit (KAPA KK8580), mRNA sequencing libraries were generated from total RNA. Magnetic oligo-dT beads captured mRNA, which was then sheared to approximately 300–350bp using heat and magnesium. The 1st strand of the mRNA fragments was reverse transcribed using random priming. The 2nd strand was generated with incorporated dUTP molecules to allow for strand-specificity. Illumina-compatible adapters with unique indexes (IDT #00989130v2) were ligated on each sample individually. The adapter ligated molecules were amplified for 10 cycles with Kapa's HIFI enzyme (KAPA KK2502). Fragment size was verified to be 450-500bp on an Agilent Tapestation and quantified with a Qubit before multiplex pooling and sequencing a 2 × 150 flow cell on the Illumina NovaSeq6000 platform at the University of Colorado Anschutz Medical Campus Genomics Core facility.

Fastq reads received from the Genomics Core were quality checked with FastQC and quality metrics were summarized with MultiQC. All samples were aligned to the mm10 mouse reference genome from Ensembl using the STAR alignment software. Gene counts were obtained using StringTie and analyzed for statistically significant differences using edgeR and DESeq2, R packages designed for RNA sequencing experiments. Clustering of samples using differentially expressed genes was also performed in R. Genes identified by any of the three tools were used to search for ontological terms in the GO and KEGG databases via weighted analysis with gProfiler and unweighted analysis with clusterProfiler on R.

3.10. MTT assay

Cell proliferation was determined using MTT reagent. Specifically, YUMM1.1 cells were cultured in DMEM/F-12 (1:1) with L-glutamine supplemented with 10% fetal bovine serum and 1% penicillin-streptomycin. Briefly, cells were seeded in flat-bottomed 96-well plates (10,000 cells per well) overnight. On the day of the treatment, PLX4720 with varying concentrations were added to YUMM1.1. Equal volume of DMEM/F-12 (1:1) was added in the no-treatment group as negative control. For positive control (all dead cells), media from wells was aspirated and methanol was added to the wells for 15 min, ensuring the death of all cells in the well, following which methanol was siphoned off and an adequate amount of media was re-added to the wells. After 48 h, 10 μL of the MTT solution was added to all wells, and the plates were placed at 37 °C for 3 h in the dark. Supernatants from all the wells were aspirated and 50 μL of DMSO:Methanol (1:1) was added to all wells following which the plates were placed in the dark at 37 °C ensuring delicate stirring of the plates. The number of viable cells was determined by measuring absorbance at 570 nm with a reference wavelength of 670 nm using a plate reader (Speedmax M2e, Sunnyvale, CA).

3.11. Flow cytometry

Flow cytometry (FACS) staining buffer was prepared by generating 0.1% bovine serum albumin (VWR, Radnor, PA), 2 mM Na_2EDTA (VWR, Radnor, PA) and 0.01% NaN_3 (VWR, Radnor, PA). Live/dead staining was performed using fixable dye eF780 (ThermoFisher Scientific, Waltham, MA, USA). All antibodies required for staining were purchased and used as is (BD biosciences, Tonbo Biosciences, BioLegend, Thermo Scientific, Invitrogen). Flow cytometry was performed by following the manufacturer's recommendation and guidelines set by ASU flow cytometry core using Attune NXT Flow cytometer (ThermoFisher Scientific, Waltham, MA, USA). Specifically, for *in vitro* experiments, cell supernatant was removed and the cells were washed in the FACS buffer, whereas for cells isolated from mice, were washed with FACS buffer once after seeding them in round-bottom 96 well plates. Next, the cells were incubated for 15 min at 4 °C in dark with 50 μL Fc Block cocktail (1 μL Fc Block + 50 μL FACS Buffer). Next, the cells were washed 1x with FACS Buffer by centrifuging at 4 °C in at 300xGs for 5 min. Next, a cocktail of 50 μL of antibodies was added to the wells, and the cells were suspended, and then incubate for 30 min at 4 °C in dark. The antibodies were used at concentrations of 0.1–1 μg/mL, per the recommendation of the manufacturer. The reagents and antibodies used in the study are as follows.

	Target	Fluorophore	Company	Catalog #	Clone
1	CD4	PE	BD	12-0041-82	GK1.5
2	CD8	APC-R700	BD	564,983	53–6.7
3	CD25	PECy7	BD	552,880	PC61
4	CD11c	PE	BioLegend	117,308	N418
5	CD86	SB600	Thermo	63-0862-82	GL1
6	CD80	PE-Cy5	Invitrogen	15-0801-82	16-10A1
7	MHCII	APC	BioLegend	107,614	M5/114.15.2
8	Tbet	BV785	BioLegend	644,835	4B10
9	FoxP3	eF450	Invitrogen	48-5773-82	FJK-16s
10	RORgT	BV650	BD	564,722	Q31-378
11	Ki67	FITC	Invitrogen	11-5698-82	SolA15
12	GATA3	BV711	BD	565,449	L50-823
13	CD16/CD32: Fc Block	NA	Tonbo	70-0161-M001	2.4G2
14	F4/80	BV702	Invitrogen	67-4801-80	BM8

(*continued on next page*)

(*continued*)

	Target	Fluorophore	Company	Catalog #	Clone
15	Comp beads	NA	Invitrogen	01-2222-42	NA
16	L/D	eF780	NA	NA	NA
17	CD11b	FITC	Tonbo	35-0112-U500	M1/70
18	CD28	NA	Tonbo	70-0281-U100	37.51
25	CD163	SB436	ThermoFisher	62-1631-82	TNKUPJ
27	CD206	PECy7	ThermoFisher	25-2061-82	MR6F3

3.12. Tumor induction and treatment for aging mouse model

Female C57BL/6j mice, >18 months old and age-matched, were used for the aging mice study. Specifically, melanoma cell line, YUMM1.1 were cultured for up to 10 passages and utilized for these studies. For inoculation, YUMM1.1 cells were counted and resuspended in either (i) sterile PBS, (ii) sterile PBS containing soluble succinate 1 mg/100 μL or (iii) sterile PBS containing 1 mg/100 μL (>20 μm) PLGA MPs or (iv) sterile PBS containing 1 mg/100 μL (>20 μm) PES MPs to obtain a solution of 7.5×10^6 cells/mL. Finally, each mouse was s. c. Injected on either side with either (i) and (iii) or (ii) and (iii). Mice were intraperitoneally injected with 20 mg/kg PLX4720 (unless otherwise mentioned) on day 21, 23, 26, 28 and 30. Mice weight and tumor growth were measured and recorded every other day. Tumor growth was measured using a digital caliper and calculated as (longest length*narrowest length^2)/2.

4. Statistics

Statistical analysis calculations were carried out using Microsoft Excel and GraphPad Prism software 9.0. For each of the experiment, statistical analysis was performed separately. p-values <0.05 was considered statistically significant. All data is expressed in the form of mean ± standard error unless otherwise specified.

Author contributions

SI designed and performed experiments, analyzed data, and wrote the manuscript; NDN and AS assisted in cell culture and material characterization; APS and JLM performed animal experiments and cell culture; HSB and MDG performed polymer characterization via NMR spectroscopy and SEC and helped with manuscript editing; JRY performed confocal microscopy; STL, XS, TH and HG performed metabolomics experiments, TK performed HPLC experiments, TER and MC assisted with extracellular flux assays; APA designed experiments and wrote the manuscript.

Declaration of competing interest

The authors declare the following financial interests/personal relationships which may be considered as potential competing interests:

Abhinav P. Acharya reports was provided by National Institutes of Health. Abhinav P. Acharya reports was provided by National Science Foundation. Abhinav P. Acharya has patent pending to Arizona State University.

Data availability

Data will be made available on request.

Acknowledgements

The authors would like to acknowledge the Flow Cytometry Core, the Regenerative Medicine Imaging Facility, the KED Genomics Core, Bioinformatics Core, the FEI at Erying Materials Center, the Advanced Light Microscopy Facilities, and the Department of Animal Care and Technologies at Arizona State University. Additionally, the authors would like to thank Dr. Seo, School of Molecular Sciences, Arizona State University for providing access to dynamic light scatter. Funding: The authors would also like to acknowledge the start-up funds provided by Arizona State University, and NIH 1R01AI155907-01, NIH 1R01AR078343-01, NIH 1R01GM144966-01, NSF award 2145877 to APA for the completion of this study. HSB and MDG would like to thank the NSF (Award# 1836719) and ARPA-E (DE-AR0001103) for funding.

Appendix A. Supplementary data

Supplementary data to this article can be found online at https://doi.org/10.1016/j.biomaterials.2023.122292.

References

[1] A. Luengo, D.Y. Gui, M.G. Vander Heiden, Targeting metabolism for cancer therapy, Cell Chem. Biol. 24 (2017) 1161–1180, https://doi.org/10.1016/j.chembiol.2017.08.028.

[2] M. Cerezo, S. Rocchi, Cancer cell metabolic reprogramming: a keystone for the response to immunotherapy, Cell Death Dis. 11 (2020) 964, https://doi.org/10.1038/s41419-020-03175-5.

[3] N. Pacifici, A. Bolandparvaz, J.S. Lewis, Stimuli-responsive biomaterials for vaccines and immunotherapeutic applications, Adv. Ther. 3 (2020), 2000129, https://doi.org/10.1002/adtp.202000129.

[4] J. Nam, S. Son, K.S. Park, J.J. Moon, Modularly programmable nanoparticle vaccine based on polyethyleneimine for personalized cancer immunotherapy, Adv. Sci. 8 (2021), 2002577, https://doi.org/10.1002/advs.202002577.

[5] S.I. Grivennikov, F.R. Greten, M. Karin, Immunity, inflammation, and cancer, Cell 140 (2010) 883–899, https://doi.org/10.1016/j.cell.2010.01.025.

[6] D.I. Gabrilovich, S. Ostrand-Rosenberg, V. Bronte, Coordinated regulation of myeloid cells by tumours, Nat. Rev. Immunol. 12 (2012) 253–268, https://doi.org/10.1038/nri3175.

[7] J. Condeelis, J.W. Pollard, Macrophages: obligate partners for tumor cell migration, invasion, and metastasis, Cell 124 (2006) 263–266, https://doi.org/10.1016/j.cell.2006.01.007.

[8] R. Noy, J.W. Pollard, Tumor-associated macrophages: from mechanisms to therapy, Immunity 41 (2014) 49–61, https://doi.org/10.1016/j.immuni.2014.06.010.

[9] C. Engblom, C. Pfirschke, M.J. Pittet, The role of myeloid cells in cancer therapies, Nat. Rev. Cancer 16 (2016) 447–462, https://doi.org/10.1038/nrc.2016.54.

[10] C.H. Ries, M.A. Cannarile, S. Hoves, J. Benz, K. Wartha, V. Runza, F. Rey-Giraud, L. P. Pradel, F. Feuerhake, I. Klaman, T. Jones, U. Jucknischke, S. Scheiblich, K. Kaluza, I.H. Gorr, A. Walz, K. Abiraj, P.A. Cassier, A. Sica, C. Gomez-Roca, K. E. de Visser, A. Italiano, C. Le Tourneau, J.-P. Delord, H. Levitsky, J.-Y. Blay, D. Rüttinger, Targeting tumor-associated macrophages with anti-CSF-1R antibody reveals a strategy for cancer therapy, Cancer Cell 25 (2014) 846–859, https://doi.org/10.1016/j.ccr.2014.05.016.

[11] A. Kulkarni, V. Chandrasekar, S.K. Natarajan, A. Ramesh, P. Pandey, J. Nirgud, H. Bhatnagar, D. Ashok, A.K. Ajay, S. Sengupta, A designer self-assembled supramolecule amplifies macrophage immune responses against aggressive cancer, Nat. Biomed. Eng. 2 (2018) 589–599, https://doi.org/10.1038/s41551-018-0254-6.

[12] S. Inamdar, T. Tylek, A. Thumsi, A.P. Suresh, M.M.C.S. Jaggarapu, M. Halim, S. Mantri, A. Esrafili, N.D. Ng, E. Schmitzer, K. Lintecum, C. de A´vila, J.D. Fryer, Y. Xu, K.L. Spiller, A.P. Acharya, Biomaterial mediated simultaneous delivery of spermine and alpha ketoglutarate modulate metabolism and innate immune cell phenotype in sepsis mouse models, Biomaterials 293 (2023), 121973, https://doi.org/10.1016/j.biomaterials.2022.121973.

[13] S. Mahbub, C.R. Deburghgraeve, E.J. Kovacs, Advanced age impairs macrophage polarization, J. Interferon Cytokine Res. 32 (2012) 18–26, https://doi.org/10.1089/jir.2011.0058.

[14] J. Leibovici, O. Itzhaki, T. Kaptzan, E. Skutelsky, J. Sinai, M. Michowitz, R. Asfur, A. Siegal, M. Huszar, G. Schiby, Designing ageing conditions in tumour microenvironment—a new possible modality for cancer treatment, Mech. Ageing Dev. 130 (2009) 76–85, https://doi.org/10.1016/j.mad.2008.03.004.

[15] N.M. Anderson, P. Mucka, J.G. Kern, H. Feng, The emerging role and targetability of the TCA cycle in cancer metabolism, Protein Cell 9 (2018) 216–237, https://doi.org/10.1007/s13238-017-0451-1.

[16] G.M. Tannahill, A.M. Curtis, J. Adamik, E.M. Palsson-Mcdermott, A.F. McGettrick, G. Goel, C. Frezza, N.J. Bernard, B. Kelly, N.H. Foley, L. Zheng, A. Gardet, Z. Tong, S.S. Jany, S.C. Corr, M. Haneklaus, B.E. Caffrey, K. Pierce, S. Walmsley, F. C. Beasley, E. Cummins, V. Nizet, M. Whyte, C.T. Taylor, H. Lin, S.L. Masters,

E. Gottlieb, V.P. Kelly, C. Clish, P.E. Auron, R.J. Xavier, L.A.J. O'Neill, Succinate is an inflammatory signal that induces IL-1β through HIF-1α, Nature (2013) https://doi.org/10.1038/nature11986.
[17] J. Connors, N. Dawe, J. Van Limbergen, The role of succinate in the regulation of intestinal inflammation, Nutrients 11 (2018) 25, https://doi.org/10.3390/nu11010025.
[18] K.J. Harber, K.E. de Goede, S.G.S. Verberk, E. Meinster, H.E. de Vries, M. van Weeghel, M.P.J. de Winther, J. Van den Bossche, Succinate is an inflammation-induced immunoregulatory metabolite in macrophages, Metabolites 10 (2020) 372, https://doi.org/10.3390/metabo10090372.
[19] C. Nastasi, A. Willerlev-Olsen, K. Dalhoff, S.L. Ford, A.-S.Ø. Gadsbøll, T.B. Buus, M. Gluud, M. Danielsen, T. Litman, C.M. Bonefeld, C. Geisler, N. Ødum, A. Woetmann, Inhibition of succinate dehydrogenase activity impairs human T cell activation and function, Sci. Rep. 11 (2021) 1458, https://doi.org/10.1038/s41598-020-80933-7.
[20] G.L. Semenza, Regulation of oxygen homeostasis by hypoxia-inducible factor 1, Physiology 24 (2009) 97–106, https://doi.org/10.1152/physiol.00045.2008.
[21] E. Monferrer, S. Sanegre, I. Vieco-Martí, A. Lo´pez-Carrasco, F. Farin˜as, A. Villatoro, S. Abanades, S. Man˜es, L. de la Cruz-Merino, R. Noguera, T. A´lvaro Naranjo, Immunometabolism modulation in therapy, Biomedicines 9 (2021) 798, https://doi.org/10.3390/biomedicines9070798.
[22] C. Rosales, E. Uribe-Querol, Phagocytosis: a fundamental process in immunity, BioMed Res. Int. (2017), https://doi.org/10.1155/2017/9042851, 2017) 9042851–9042851.
[23] Y.-P. Wang, Q.-Y. Lei, Metabolite sensing and signaling in cell metabolism, Signal Transduct. Targeted Ther. 3 (2018) 30, https://doi.org/10.1038/s41392-018-0024-7.
[24] Q. Wei, Y. Qian, J. Yu, C.C. Wong, Metabolic rewiring in the promotion of cancer metastasis: mechanisms and therapeutic implications, Oncogene 39 (2020) 6139–6156, https://doi.org/10.1038/s41388-020-01432-7.
[25] B. Kelly, L.A. O'Neill, Metabolic reprogramming in macrophages and dendritic cells in innate immunity, Cell Res. 25 (2015) 771–784, https://doi.org/10.1038/cr.2015.68.
[26] L.L. Cunha, S.F. Perazzio, J. Azzi, P. Cravedi, L.V. Riella, Remodeling of the immune response with aging: immunosenescence and its potential impact on COVID-19 immune response, Front. Immunol. 11 (2020), https://doi.org/10.3389/fimmu.2020.01748.
[27] A.C. Shaw, D.R. Goldstein, R.R. Montgomery, Age-dependent dysregulation of innate immunity, Nat. Rev. Immunol. 13 (2013) 875–887.
[28] Z. Huang, B. Chen, X. Liu, H. Li, L. Xie, Y. Gao, R. Duan, Z. Li, J. Zhang, Y. Zheng, Effects of sex and aging on the immune cell landscape as assessed by single-cell transcriptomic analysis, Proc. Natl. Acad. Sci. USA 118 (2021).
[29] P. Kelly, R. Davison, E. Bliss, J. McGee, Macrophages in human breast disease: a quantitative immunohistochemical study, Br. J. Cancer 57 (1988) 174–177.
[30] C.H. Kugel, S.M. Douglass, M.R. Webster, A. Kaur, Q. Liu, X. Yin, S.A. Weiss, F. Darvishian, R.N. Al-Rohil, A. Ndoye, R. Behera, G.M. Alicea, B.L. Ecker, M. Fane, M.J. Allegrezza, N. Svoronos, V. Kumar, D.Y. Wang, R. Somasundaram, S. Hu-Lieskovan, A. Ozgun, M. Herlyn, J.R. Conejo-Garcia, D. Gabrilovich, E.L. Stone, T. S. Nowicki, J. Sosman, R. Rai, M.S. Carlino, G.V. Long, R. Marais, A. Ribas, Z. Eroglu, M.A. Davies, B. Schilling, D. Schadendorf, W. Xu, R.K. Amaravadi, A. M. Menzies, J.L. McQuade, D.B. Johnson, I. Osman, A.T. Weeraratna, Age correlates with response to anti-PD1, reflecting age-related differences in intratumoral effector and regulatory T-cell populations, Clin. Cancer Res. 24 (2018) 5347–5356, https://doi.org/10.1158/1078-0432.CCR-18-1116.
[31] A. Kaur, M.R. Webster, K. Marchbank, R. Behera, A. Ndoye, C.H. Kugel, V.M. Dang, J. Appleton, M.P. O'Connell, P. Cheng, A.A. Valiga, R. Morissette, N.B. McDonnell, L. Ferrucci, A.V. Kossenkov, K. Meeth, H.-Y. Tang, X. Yin, W.H. Wood, E. Lehrmann, K.G. Becker, K.T. Flaherty, D.T. Frederick, J.A. Wargo, Z.A. Cooper, M.T. Tetzlaff, C. Hudgens, K.M. Aird, R. Zhang, X. Xu, Q. Liu, E. Bartlett, G. Karakousis, Z. Eroglu, R.S. Lo, M. Chan, A.M. Menzies, G.V. Long, D.B. Johnson, J. Sosman, B. Schilling, D. Schadendorf, D.W. Speicher, M. Bosenberg, A. Ribas, A. T. Weeraratna, sFRP2 in the aged microenvironment drives melanoma metastasis and therapy resistance, Nature 532 (2016) 250–254, https://doi.org/10.1038/nature17392.
[32] A.P. Acharya, N.V. Dolgova, M.J. Clare-Salzler, B.G. Keselowsky, Adhesive substrate-modulation of adaptive immune responses, Biomaterials (2008), https://doi.org/10.1016/j.biomaterials.2008.08.040.
[33] J.D. Fisher, W. Zhang, S.C. Balmert, A.M. Aral, A.P. Acharya, Y. Kulahci, J. Li, H. R. Turnquist, A.W. Thomson, M.G. Solari, V.S. Gorantla, S.R. Little, In situ recruitment of regulatory T cells promotes donor-specific tolerance in vascularized composite allotransplantation, Sci. Adv. (2020), https://doi.org/10.1126/sciadv.aax8429.
[34] J.D. Fisher, S. Balmert, W. Zhang, R. Schweizer, J.T. Schnider, C. Komatsu, L. Dong, V.E. Erbas, J.V. Unadkat, A. Aral, A.P. Acharya, Y. Kulahci, H. R. Turnquist, A.W. Thomson, M.G. Solari, V.S. Gorantla, S.R. Little, Treg-inducing microparticles promote donor-specific tolerance in experimental vascularized composite allotransplantation, Proc. Natl. Acad. Sci. USA 116 (51) (2019) 25784–25789, https://doi.org/10.1073/pnas.1910701116.
[35] E. Mills, L.A.J. O'Neill, Succinate: a metabolic signal in inflammation, Trends Cell Biol. 24 (2014) 313–320, https://doi.org/10.1016/j.tcb.2013.11.008.
[36] M. Binnewies, E.W. Roberts, K. Kersten, V. Chan, D.F. Fearon, M. Merad, L. M. Coussens, D.I. Gabrilovich, S. Ostrand-Rosenberg, C.C. Hedrick, R. H. Vonderheide, M.J. Pittet, R.K. Jain, W. Zou, T.K. Howcroft, E.C. Woodhouse, R. A. Weinberg, M.F. Krummel, Understanding the tumor immune microenvironment (TIME) for effective therapy, Nat. Med. 24 (2018) 541–550, https://doi.org/10.1038/s41591-018-0014-x.
[37] D. Gong, W. Shi, S. Yi, H. Chen, J. Groffen, N. Heisterkamp, TGFβ signaling plays a critical role in promoting alternative macrophage activation, BMC Immunol. 13 (2012) 1–10.
[38] D.J. Huss, R.C. Winger, H. Peng, Y. Yang, M.K. Racke, A.E. Lovett-Racke, TGF-β enhances effector Th1 cell activation but promotes self-regulation via IL-10, J. Immunol. 184 (2010) 5628–5636.
[39] M.T. Wolf, S. Ganguly, T.L. Wang, C.W. Anderson, K. Sadtler, R. Narain, C. Cherry, A.J. Parrillo, B.V. Park, G. Wang, F. Pan, S. Sukumar, D.M. Pardoll, J.H. Elisseeff, A biologic scaffold–associated type 2 immune microenvironment inhibits tumor formation and synergizes with checkpoint immunotherapy, Sci. Transl. Med. 11 (2019), eaat7973, https://doi.org/10.1126/scitranslmed.aat7973.
[40] I. Xhangolli, B. Dura, G. Lee, D. Kim, Y. Xiao, R. Fan, Single-cell analysis of CAR-T cell activation reveals A mixed TH1/TH2 response independent of differentiation, Dev. Reprod. Biol. 17 (2019) 129–139, https://doi.org/10.1016/j.gpb.2019.03.002.
[41] Y. Kaiser, R. Lepzien, S. Kullberg, A. Eklund, A. Smed-So¨rensen, J. Grunewald, Expanded lung T-bet + RORγT + CD4 + T-cells in sarcoidosis patients with a favourable disease phenotype, Eur. Respir. J. 48 (2016) 484–494, https://doi.org/10.1183/13993003.00092-2016.
[42] Y. Wang, J. Godec, K. Ben-Aissa, K. Cui, K. Zhao, A.B. Pucsek, Y.K. Lee, C. T. Weaver, R. Yagi, V. Lazarevic, The transcription factors T-bet and runx are required for the ontogeny of pathogenic interferon-γ-producing T helper 17 cells, Immunity 40 (2014) 355–366, https://doi.org/10.1016/j.immuni.2014.01.002.
[43] A.P. Acharya, N.V. Dolgova, C.Q. Xia, M.J. Clare-Salzler, B.G. Keselowsky, Adhesive substrates modulate the activation and stimulatory capacity of non-obese diabetic mouse-derived dendritic cells, Acta Biomater. (2011), https://doi.org/10.1016/j.actbio.2010.08.026.
[44] A.P. Acharya, M.R. Carstens, J.S. Lewis, N. Dolgova, C.Q. Xia, M.J. Clare-Salzler, B. G. Keselowsky, A cell-based microarray to investigate combinatorial effects of microparticle-encapsulated adjuvants on dendritic cell activation, J. Mater. Chem. B (2016), https://doi.org/10.1039/c5tb01754h.
[45] A.P. Acharya, M. Sinha, M.L. Ratay, X. Ding, S.C. Balmert, C.J. Workman, Y. Wang, D.A.A. Vignali, S.R. Little, Localized multi-component delivery platform generates local and systemic anti-tumor immunity, Adv. Funct. Mater. (2017), https://doi.org/10.1002/adfm.201604366.
[46] J.L. Mangal, S. Inamdar, Y. Yang, X. Shi, M. Wankhede, H. Gu, K. Rege, M. D. Green, M. Curtis, A. Acharya, Metabolite releasing polymers control dendritic cell function by modulating their energy metabolism, J. Mater. Chem. B (2020), https://doi.org/10.1039/d0tb00790k.
[47] J.L. Mangal, S. Inamdar, T. Le, X. Shi, M. Curtis, H. Gu, A.P. Acharya, Inhibition of glycolysis in the presence of antigen generates suppressive antigen-specific responses and restrains rheumatoid arthritis in mice, Biomaterials 277 (2021), 121079, https://doi.org/10.1016/j.biomaterials.2021.121079.
[48] J.L. Mangal, S. Inamdar, A.P. Suresh, M.M.C.S. Jaggarapu, A. Esrafili, N.D. Ng, A. P. Acharya, Short term, low dose alpha-ketoglutarate based polymeric nanoparticles with methotrexate reverse rheumatoid arthritis symptoms in mice and modulate T helper cell responses, Biomater. Sci. 10 (2022) 6688–6697, https://doi.org/10.1039/d2bm00415a.